

# Dark Navigation : Sensing and Rover Navigation in Permanently Shadowed Lunar Craters

Liam Pedersen<sup>1</sup>, Chin San Han<sup>2</sup>, and Michael Vitus<sup>2</sup>

<sup>1</sup>NASA Ames Research Center / Carnegie Mellon University, Moffett Field, California, USA

<sup>2</sup>NASA Ames Research Center / Stanford University, Moffett Field, California, USA

## Abstract

*Permanently shadowed lunar craters are high priority targets for future exploration because of the possibility they harbor water ice. Orbital neutron spectrometer and terrestrial radar data support this, but definitive confirmation and a detailed survey is likely to require in situ analysis by a rover.*

*Landing and navigating inside permanently shadowed craters presents a sensing challenge. We consider high dynamic range stereo images using an LED spotlight, laser triangulation, scanning lidar, and dense 3D flash lidar. Navigation hazard sensing requirements are derived from a review of the lunar crater terrain.*

*The single plane range scanners (scanning lidar and laser triangulation) require locally accurate, high bandwidth rover pose information to transform their outputs into a common reference frame within which to build 3D terrain maps. The dense 2-D range sensors (stereo, flash lidar) are limited in the range of distances they can look ahead.*

*Traversability analysis algorithms robust to the pose error induced noise in the measured 3D terrain maps are described, along with a procedure to combine them.*

*Key words: navigation; sensors; hazard detection; dark lunar craters.*

## 1. Introduction

Terrestrial radar measurements [1] of the Lunar south polar regions (Fig. 1) determined the existence of craters with permanently shadowed interiors sufficiently cold to harbor water ice. This is corroborated by the radar echoes and Lunar Prospector neutron spectrometer data that suggest localized concentrations of H<sub>2</sub>O up to 40% by weight (collected references in [2]).

The potential for water makes permanently shadowed lunar craters high priorities for exploration. The calculated H<sub>2</sub>O abundances are very uncertain, and the local distribution is unknown. NASA's

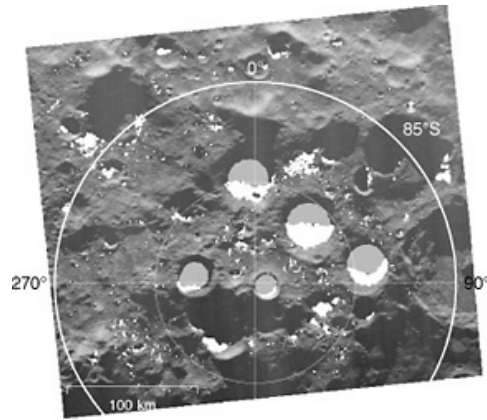


Figure 1: Radar map of the lunar south pole obtained with the 3.5cm Goldstone radar. White – areas visible to Earth but in permanent shadow. Gray – no radar return but predicted to be in permanently shadowed. ( From [1].)



Figure 2: Carnegie Mellon University's Scarab robot. Mast mounted scanning lidar sensors map the terrain for obstacle detection. (Photo: CMU)

LCROSS mission will impact a polar crater in 2009 to attempt a confirmation of H<sub>2</sub>O abundance, but

the definitive assessment of the water/hydrogen distribution in the crater floor regolith is likely to require exploration with a neutron spectrometer and drill equipped robotic rover.

Navigating a rover inside a permanently dark crater presents challenges. By definition, the craters are dark and there are no detailed (optical) images of their interior. Temperature is 100 K. Communication with Earth, either directly (where possible) or through lunar polar orbiting satellites would be intermittent.

This paper addresses the problem of detecting navigational hazards for a rover in one of the dark lunar south polar craters. Our system is designed for Carnegie Mellon University’s Scarab robot (Fig. 2), a vehicle expressly designed to deploy a drill in lunar terrain [3], but applies to any wheeled vehicle that must traverse rough terrain in darkness.

The following sections review of the lunar crater floor environment, assess likely navigation hazards and derive sensing requirements. Then follows a summary of active range sensors for terrain mapping and hazard detection, terrain traversability analysis algorithms suitable for push-broom type sensors, and future directions.

## 2. Lunar Crater Floor Navigation Hazards

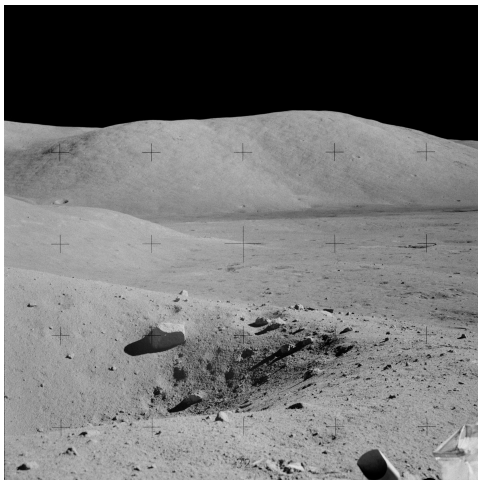


Figure 3: Ballet Crater (diameter 10m) near Lincoln Scarp investigated by Apollo 17 might represent the predominant obstacles to be found within large South polar craters such as Shackleton. Note the steep edges and excavated ejecta blocks up to 0.5m in size. (photo: NASA)

Without detailed images, navigation hazards in the permanently shadowed areas can only at present be inferred from radar circular polarization measurements which “suggest that regolith in lowly-

ing areas near the south pole is characterized by significant impact melt component from Orientale, which may explain the block rich ejecta around small craters observed in this and earlier radar studies” [4]. This, and experience from Apollo and subsequent missions to other parts of the Moon, motivates the hypothesis that the dominant navigation hazards in the south polar dark crater floors are small craters and their associated ejecta blocks, such as in Fig. 3.

Crater depth, rim height, ejecta block diameter and other parameters can be empirically modeled by  $\alpha D^\beta$  where  $D$  is the crater diameter [5](Table 1). For craters bigger than 35m we can expect 30cm ejecta blocks. For small craters, depth is approximately 20% of diameter and maximum slope  $41^\circ$  (determined with a parabola model of crater profile).

Table 1: Lunar crater empirical model parameters:  $Property = \alpha(Diameter/[m])^\beta$

Property	$\alpha$	$\beta$
Depth (m)	0.210	1.010
Rim height (m)	0.040	1.014
Rim width (m)	0.277	1.011
Max ejecta block diameter (m)	0.003	0.660
Density (craters/m <sup>2</sup> )	0.035	-2.800

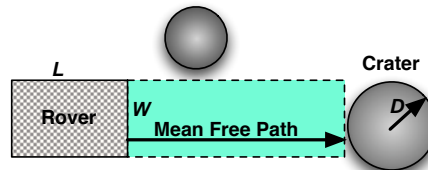


Figure 4: The *mean free path*, or average distance the rover will travel in a straight line before hitting an obstacle can be calculated by solving the following equation for  $x$  (where  $[D_{min}, D_{max}]$  is the diameter range of untraversable craters) :

$$\int_{D_{min}}^{D_{max}} (x + D/2)(W + D)p(D)dD = 1$$

Lunokhod data [6] suggest that crater areal density also depends on crater diameter as above. This can be visualized using the *mean free path* – the average distance a rover can travel before hitting an obstacle [7](Fig. 4). A Scarab sized vehicle (1.5m  $\times$  1.5m) has a mean free path of 9.5 vehicle lengths before hitting a 1.5 – 50m crater (this density model is unproven for larger craters. We expect that craters over 50 m can be mapped *a priori* by the LRO’s LOLA instrument).

This means that Scarab probably will not need to maneuver through tight spots, and can travel mostly in a straight line. Consequently, skid steering will not incur a significant energy penalty and sophisticated path planning is unnecessary.

### 3. Navigation Sensing Requirements

Isolated ejecta blocks and crater rims are presumed to constitute the primary navigation hazards on the lunar surface (Fig. 5). We call these geometric hazards, in that they are a feature of the surface geometry and thus detectable with range sensors that recover a sufficiently accurate 3D terrain map. We now consider the requirements for this terrain map.

The height  $H_{min}$  of the smallest blocks the rover cannot drive over is given by the minimum of the rover wheel radius, and the axle and body clearances. The smallest void that could entrap a wheel is about 0.7 times the wheel diameter. Large scale topographic hazards, such as crater rims and slopes are on the scale of 0.5 times the rover wheelbase. Assuming the world is smooth (no tyre spikes), the Nyquist theorem dictates the *sampling distance*  $d_{sample}$  should be  $\frac{1}{2}H_{min}$  and both the sensor footprint and precision  $\epsilon$  should be  $\frac{1}{2}d_{sample}$ . Note that the sensor sampling distance, precision and footprint requirements apply to both horizontal and vertical terrain measurements. Table 2 summarizes Scarab parameters and derived *minimum* sensor requirements. In practice it is desirable to exceed these requirements by at least a factor of 2 or more, as sensor performance will vary with terrain geometry and rover motion.

Deriving requirements for sensor look ahead distance and field of view (FOV) is less straight forward. The look ahead must be at least the minimum stopping or turning distance, and FOV sufficiently wide to encompass the rover width plus maneuvering and safety margin. See [8] for a full discussion.

Increasing the sensor look ahead and FOV beyond the mandated safety margins enables more *efficient* path planning. [9] empirically shows a trade-off between look ahead distance and *a priori* map resolution. From past experience in similarly cluttered terrain [10], we (heuristically) judge a look ahead distance of 5 – 10 m and 90° field of view to be desirable.

## 4. Terrain Sensors

Finding appropriate range sensors that determine the 3D geometry of the terrain around the rover in complete darkness whilst meeting the aforementioned requirements is key to solving this problem. Fig. 6 lists the sensors investigated.

### 4.1. Stereo vision with artificial illumination

Stereo vision is the basis of the venerable Morphin obstacle avoidance algorithm [11] and has been well established by the MER vehicles that presently operate on Mars. Besides flight heritage, the great advantage of stereo vision is that it generates a *dense* range image. A single near instantaneous measurement generates sufficient points to map the area in front of the robot.

Stereo vision easily meets the precision and sampling interval requirements, but requires an artificial light source to work in the dark. In [12] we demonstrate good results using a pulsed red LED spotlight with commercially available CCD stereo cameras. However, because of the  $1/\text{distance}^2$  fall-off in light intensity, either a 0.5 s integration time or  $36\times$  increase in peak LED power output would be needed to get 10 m look-ahead and 90° FOV. We also demonstrated that only a narrow range of distances are appropriately exposed to get good stereo matches. We solved this by combining multiple images with different exposures times into a single high dynamic range image, at the expense of requiring the vehicle to stop for each sensor update. Other options we did not investigate include projecting structured light onto the surroundings, using high dynamic range cameras or shaping the illumination.

Further disadvantages of stereo are the significant energy and time that results from the large computation required. Autonomous navigation with the MER vehicles is 3–5 times slower than blind driving for this reason.

### 4.2. Flash lidar

Flash lidar [13] [14] deliver instantaneous dense range images. We tested the CSEM SwissRanger SR3000 and a development prototype from Ball Aerospace with JSC-1AF lunar regolith simulant coated ground targets in a dark room. The SR3000 emits modulated light from a bank of LED's. Circuitry at each receiver pixel determines the phase, theoretically permitting range measurements of objects up to 8 m distant. In practice, it resolves rocks up to 5.5m away, but is subject to motion blur and requires filtering. The Ball sensor is a true time-of-flight system that can measure targets several km away with good accuracy and no blur. At present it is limited to 8° field of view and not ready for rover integration.

### 4.3. Laser triangulation

Laser triangulation works by projecting a plane of light onto the scene and detecting its displacement in an image obtained by an offset camera (Fig. 6). Great accuracy is attainable with little computation. We tested a custom unit [15] with its own em-

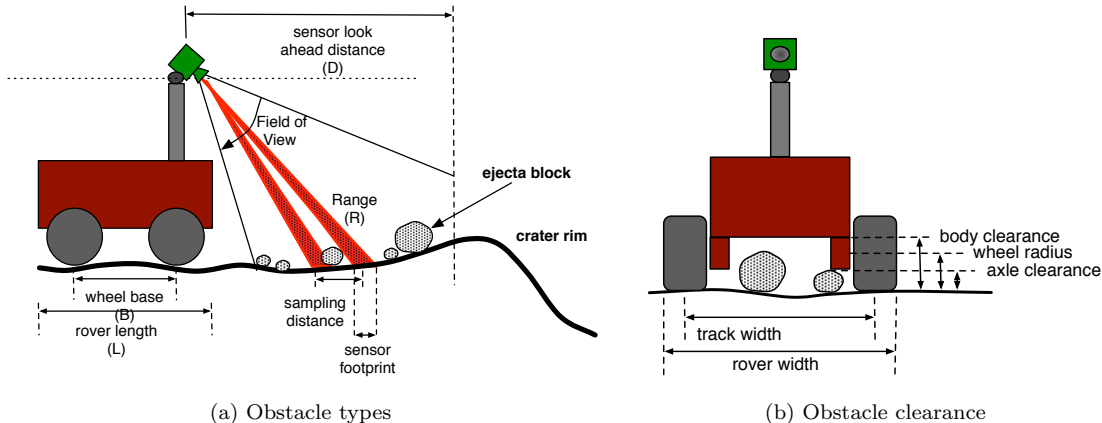


Figure 5: Hazard types, rover dimensions and mapping sensor parameters

Table 2: Conservative Scarab parameters and derived *minimum* requirements

Wheel base ( $B$ )		1.5 m
Body clearance ( $c_{body}$ )		0.3 m
Axle clearance ( $c_{axle}$ )		0.3 m
Wheel radius ( $r_{wheel}$ )		0.35 m
Minimum obstacle height ( $H_{min}$ )	$\min\{c_{body}, c_{axle}, r_{wheel}\}$	0.3 m
Minimum sampling interval ( $d_{sample}$ )	$\frac{1}{2}H_{min}$	0.15 m
Minimum sensor precision ( $\epsilon$ )	$\frac{1}{2}d_{sample}$	0.075 m
Maximum driving speed ( $v$ )		$0.10 \text{ ms}^{-1}$
Maximum reaction time ( $T_{react}$ )		1.0 s
Lunar gravity ( $g$ )		$0.1.62 \text{ ms}^{-2}$
Rover-regolith friction coefficient ( $u$ )		0.5
Minimum stopping distance ( $d_{stop}$ )	$vT_{react} + \frac{v^2}{2ug}$	0.106 m

bedded computation to maximize throughput, that has demonstrated sub-mm accuracy. Because the projected light is confined to a plane and image saturation is not an issue, its intensity fall off with distance is not an issue for this application.

The disadvantage of a laser scanner is that it only measures range to points within a single plane. To map an area the sensor must be mechanically swept across the scene, either with a gimbal or using the motion of the rover itself (in the so called “push-broom” configuration). The sensor pose history is required to transform measured points into a common mapping frame. Accumulated pose errors between readings will result in mapping errors. Rover velocity must be limited to ensure an adequate sampling interval.

#### 4.4. Scanning lidar

Many mature, turn-key time-of-flight scanning lidar systems exist that offer reasonable resolution, range and adequate scan rates. Like laser triangula-

tion, they are (mostly) confined to single plane measurements. To date, they lack flight heritage, perhaps because they contain moving parts and have hitherto been bulky.

## 5. Traversability Analysis

Laser triangulation offers the best combination of dynamic range, precision, computational economy, and ease of integration, but with the serious shortcoming that it obtains measurements only along 1 dimension. Robust analysis algorithms that can use data from this sensor in a push-broom configuration (Fig. 7), combined with Scarab’s pose estimates, would make this the sensor of choice.

We chose Hokuyo URG scanning lidars as a temporary substitute for a laser triangulation sensor currently under development. Whilst falling short of the range requirements (the maximum range is about 3.5 m in sunlight) the URG is commercially available and convenient for development.



Figure 6: Terrain hazard detection sensors

### 5.1. Morphin

Morphin [11] has an impressive autonomous navigation track record, with a recent variant GESTALT guiding the Mars rovers Spirit and Opportunity. It works by dividing the terrain into a grid of square cells. 3D terrain points acquired by sensors (usually stereo) are assigned to the closest cell. Cell traversability is determined by fitting a plane to the points in that cell, and to points in a rover sized patch surrounding that cell. Residual errors and the slope of the rover sized patch determine a traversability (or “goodness”) score, between 0 and 1, for that cell. A confidence score, also between 0 and 1, is computed based on the number of points in the cell.

Morphin was designed for use with stereo cameras. The assumption is that a dense, *consistent* set of 3D points covering the area in front of the rover can be obtained simultaneously and used to generate a single map. A new map is generated each time another stereo camera measurement is made. As stated previously, this assumption breaks down when using data from a 1-D range scanner in a push-broom configuration. In this situation, rover pose estimates are used to continuously transform sensed 3D points into a common reference frame.

Inadequate pose information can lead to discontinuities in the terrain map (Fig. 7b), and thence fictitious obstacles under Morphin (Fig. 7c). Pose estimates should not contain discontinuities and must be at a sufficiently high update rate to capture vehicle dynamics, especially pitch oscillations. Pose errors are tolerable if the *relative* errors between updates are small to limit pose error induced map ripples in a grid cell to less than the minimum required mapping precision ( $\epsilon$ ) indicated in Table 2 less sensor precision.

### 5.2. Other Approaches

In practice it is hard to meet the pose information quality requirements, particularly when looking far ahead or moving rapidly. Stanford University’s Stanley vehicle solved this problem by labeling any discontinuity in perceived terrain elevation above a dynamically determined threshold as an obstacle [16]. By linking this threshold to estimated relative pose errors Stanley was able to disambiguate between real and fictitious obstacles with sufficient accuracy to win the 2006 Darpa Grand Challenge (DPG) using laser scanners for obstacle detection. The drawback of this algorithm is that it does not directly measure slope and so is unlikely to cor-

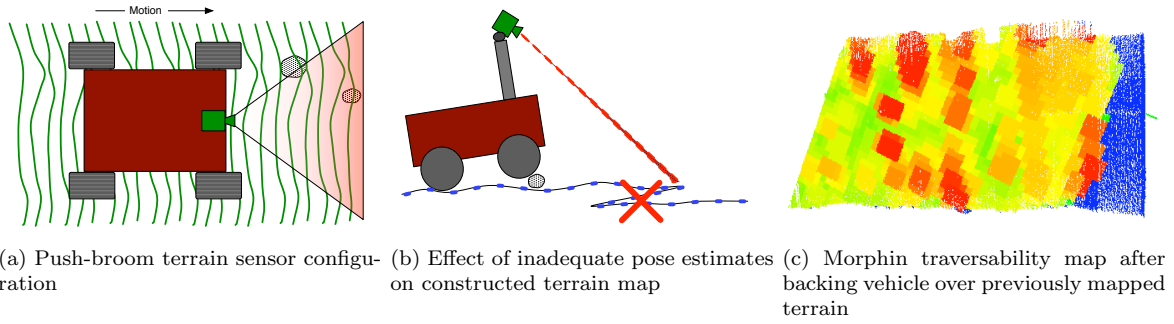


Figure 7: Effects of inadequate pose information when attempting to use Morphin with a push-broom type range sensor

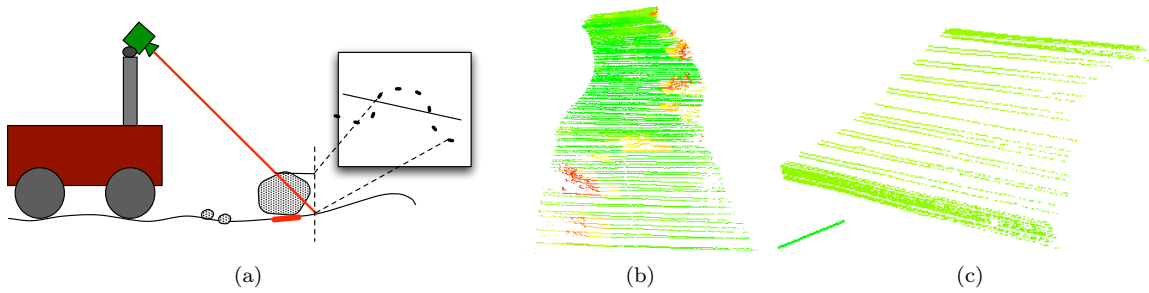


Figure 8: The Projected Line Fit algorithm (a) clearly identifies isolated obstacles (b) but fails to correctly label a berm (c) directly in front of the vehicle as hazardous

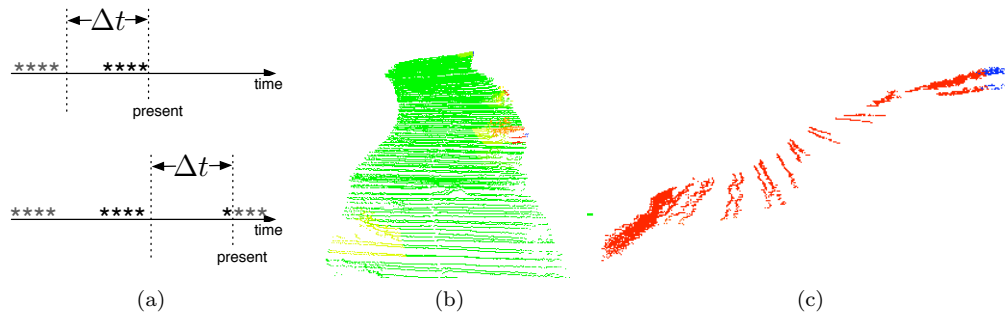


Figure 9: Time Windowed Morphin (a) misses some isolated obstacles (b) that are identified by PLF (Fig. 8b) but correctly labels large features such as the hazardous berm (c) that PLF misses (Fig. 8c)

rectly flag large but smooth topographic features (like crater rims) as hazardous.

Carnegie Mellon University’s Highlander and Sandstorm 2006 DPG entrants employed a different approach [17], which we call *Projected Line Fit* (PLF)(Fig. 8) that calculates traversability scores from single line scans at a time. As the name implies, it works by projecting the scan points onto a vertical plane and fitting a line to them. A large residual, or steep angle with the horizontal indicate an obstacle. PLF is easier to implement than the Stanley algorithm (requiring fewer parameters, that in Stanley’s case must be learned from data) but would miss obstacles that only show up as changes between scans – for example a berm parallel to the scan direction (Fig. 8c).

A third approach that we developed, called *Time-Windowed Morphin* (TWM) stems from the observations that terrain points obtained close together in time are usually consistent, and that points close together in space are likely to have been obtained close together in time. TWM works like Morphin, but only uses the most recent terrain data points within  $\Delta t$  of each other to calculate the best plane fits, with care taken to not overwrite old traversability and certainty scores until sufficient new data is obtained (Fig. 9a).

Unlike Morphin (Fig. 7c), TWM correctly re-labels previously traversed terrain as traversable. With appropriately loose thresholds on plane fit residuals TWM can be robust to small pose errors induced by vehicle shaking. Whilst this is at the expense of not detecting small obstacles (Fig. 9b), berms and large terrain features missed by PLF are detected (Fig. 9c).

### 5.3. Combining Traversability Maps

Without a single approach capable of detecting all hazards yet robust to pose information inadequacies, it is necessary to merge hazard maps from multiple algorithms. The obvious, if ad hoc, approach is a weighted average of cell traversabilities, using the certainty values as weights. This has been successfully used to merge successive Morphin maps [18] and to merge maps from different sensors [17].

The trouble with a weighted average stems from the nature of the certainty value, which is usually derived from the number of points used to make an evaluation, and is not necessarily a true measure of confidence. In the examples above, both PLF and TWM mislabel hazards with high certainty. As they detect different hazards, an average value will wash them out.

A more correct way to merge maps, inspired by the occupancy grid approach [19] is to treat the traversability score  $\theta_i$  from each method  $i$  as been statistically conditioned on whether the map cell is indeed traversable or not:

$$p(\text{trav}|\theta_i) = \frac{p(\theta_i|\text{trav})p(\text{trav})}{p(\theta_i)} \quad (1)$$

Assuming that the methods are conditionally independent given a cells traversability, we get:

$$p(\text{trav}|\theta_j, \theta_i) = \frac{p(\theta_j|\text{trav})p(\text{trav}|\theta_i)}{p(\theta_j)} \quad (2)$$

This requires statistically characterizing each method, a time consuming data intensive task, and the above assumption is not necessarily valid.

Our approach is predicated on the observation that TWM and PLF are both more likely to be correct when they detect a hazard. If they both return results that exceed a certainty threshold, we pick the most pessimistic (lowest) traversability score. If neither do, we also choose the lowest. If only one returns a result with confidence, we pick that.

## 6. Conclusions and Further Work

Laser triangulation in a push-broom configuration at present appears the best sensing modality for navigation a rover inside a permanently shadowed lunar crater – provided reasonably high rate pose estimates and traversability analysis algorithms robust to pose error induced artifacts are available.

We introduce TWM, a modification of the Morphin algorithm and show how to combine it with other algorithms to get a (conservative) map of lunar navigation hazards using a push-broom type sensor. Results shown so far use scanning lidar data from the K-10 and Zoe vehicles. There is an ongoing effort to mount sensors on the Scarab vehicle and demonstrate the complete system in December 2007.

Flash lidar, especially time-of-flight systems are *very* promising for this application. Work remains to mature the prototypes for rover integration and widen the field of view (or introduce a scanning mechanism).

## Acknowledgment

The authors would like to thank David Wettergreen and Dominic Jonak of Carnegie Mellon University. This project was supported by the NASA Exploration Technology Development Program (Human-Robotic Systems Project). Chin San Han and Michael Vitus are supported at NASA Ames through NASA’s Educational Associates program.

## References

1. Margot, J., Campbell, D., Jurgens, R., and Slade, M. Topography of the lunar poles from

- radar interferometry: a survey of cold trap locations. *Science*, 284:1658–1660, June 1999.
2. Allen, C. Shoemaker crater - going where we can "see". Lcross site selection, NASA Johnson Space Center, NASA Johnson Space Center, Mail Code KT, Houston, TX 77058, 2006.
  3. Bartlett, P., Wettergreen, D., and Whittaker, W. L. Design of the scarab rover for mobility and drilling in the lunar cold traps. In *International Symposium on Artificial Intelligence, Robotics and Automation in Space (iSAIRAS)*, Los Angeles, California, February 2008.
  4. Campbell, B. A. and Campbell, D. B. Regolith properties in the south polar region of the moon from 70-cm radar polarimetry. *Icarus*, January 2006.
  5. Heiken, G. H., Vaniman, D. T., and French, B. M., editors. *Lunar sourcebook - a user's guide to the moon*. Cambridge University Press, 1991.
  6. Vinogradov, A. A. P., editor. *Lunokhod-1 Mobile Lunar Laboratory, USSR (Peredvizhnaya Laboratoriya na Lune Lunokhod-1)*. Number 54525. US Department of Commerce Joint Publications Research Service, Moscow, 4 June 1971.
  7. Wilcox, B., Nasif, A., and Welch, R. Implications of martian rock distributions on rover scaling. *Space Technology*, 1997.
  8. Kelly, A. and Stentz, A. Rough terrain autonomous mobility-part 1: A theoretical analysis of requirements". *Autonomous Robots*, 5:129–161, 1998.
  9. Urmson, C. *Navigation Regimes for Off-Road Autonomy*. PhD thesis, Robotics Institute, Carnegie Mellon University, May 2005.
  10. Bualat, M., Edwards, L., Fong, T., Broxton, M., Flueckiger, L., Lee, S. Y., Park, E., To, V., Utz, H., Verma, V., Kunz, C., and MacMahon, M. Autonomous robotic inspection for lunar surface operations. In *International Conference on Field and Service Robotics (FSR)*, 6, Chamonix, France, July 9-12 2007.
  11. Simmons, R., Henriksen, L., Chrisman, L., and Whelan, G. Obstacle avoidance and safeguarding for a lunar rover. In *AIAA Forum on Advanced Developments in Space Robotics*, Madison, WI, 1996.
  12. Husmann, K. and Pedersen, L. Strobe lit high dynamic range stereo imagery for dark navigation. In *International Symposium on Artificial Intelligence, Robotics and Automation in Space (iSAIRAS)*, 2008.
  13. Anderson, D., Herman, H., and Kelly, A. Experimental characterization of commercial flash ladar devices. In *International Conference on Sensing Technologies*, Palmerston North, New Zealand, November 2005.
  14. Craig, R., Gravseth, I., Earhart, R. P., Blatt, J., Barnhill, S., Ruppert, L., and Centamore, C. Processing 3D flash LADAR point-clouds in real-time for flight applications. In *Sensors and Systems for Space Applications. Edited by Howard, Richard T.; Richards, Robert D. Proceedings of the SPIE, Volume 6555, pp. 65550D (2007)*, volume 6555 of *Presented at the Society of Photo-Optical Instrumentation Engineers (SPIE) Conference*, May 2007.
  15. Bualat, M., Kunz, C., Lavelle, J., Pedersen, L., and Schuet, S. Scanning laser rangefinder for accurate arm placement and inspection. In *International Symposium on Artificial Intelligence, Robotics and Automation in Space (iSAIRAS)*, Munich, Germany, September 2005.
  16. Thrun, S., Montemerlo, M., and Aron, A. Probabilistic terrain analysis for high speed desert driving. In Sukhatme, G., Schaal, S., Burgard, W., and Fox, D., editors, *Robotics Science and Systems Conference*, Philadelphia, PA, 2006.
  17. Urmson, C., Anhalt, J., Bartz, D., Clark, M., Galatali, T., Gutierrez, A., Harbaugh, S., Johnston, J., Kato, H., Koon, P. L., Messner, W., Miller, N., Mosher, A., Peterson, K., Ragusa, C., Ray, D., Smith, B. K., Snider, J. M., Spiker, S., Struble, J. C., Ziglar, J., and Whittaker, W. R. L. A robust approach to high-speed navigation for unrehearsed desert terrain. *Journal of Field Robotics*, 23(8):467–508, August 2006.
  18. Singh, S., Simmons, R., Smith, T., Stentz, A., Verma, V., Yahja, A., and Schwehr, K. Recent progress in local and global traversability for planetary rovers. In *IEEE International Conference on Robotics and Automation*, San Francisco, April 2000. IEEE.
  19. Elfes, A. Sonar-based real-world mapping and navigation. *IEEE Journal of Robotics and Automation*, RA-3(3):249–265, June 1987.